

# Design and Experimental Investigation of Four-Bar Dynamic Testing Machine

MUHAMMAD MAARIJ<sup>1</sup>, MUHAMMAD ALI<sup>2</sup>, MUHAMMAD SHEHRYAR MANZOOR<sup>3</sup>

Mechanical Engineering Department,  
University of Engineering and Technology,  
Taxila,  
PAKISTAN

<sup>1</sup> 0000-0001-8153-567X

*Abstract:* - This project involved fabricating and experimental investigation of a dynamic testing machine for four-bar mechanisms with various applications. The simple crank rocker inversion is selected, and the kinematic design of the four-bar mechanism is done by keeping in view the Grashof rotatability criteria and the dynamic design required factoring in the forces acting on various links. The flywheel is designed to minimize the fluctuations in the torque required to drive the mechanism. DE-ASME Elliptic criteria is used for the shaft design and selection of bearing. For transmitting power from the AC motor to the crankshaft, a V belt and a pulley are used as the belt helps dampen the vibration effects in the mechanism. The linkages were fabricated, and the mechanism was assembled. ADXL335 accelerometer sensor is mounted on the apparatus to measure the acceleration of a point on the coupler. This acceleration data was then integrated using numerical techniques to estimate velocity and displacement. The model changes can be adjusted according to the dimensions of the bars and angles between the bars to simulate the performance of the mechanism. Due to the inherent offset in the sensor, an error was included in the data. However, the results obtained using such methods were satisfactory in visualizing the behaviour of data representing the system's motion under running conditions. The errors in the result can be minimized using more advanced integration techniques and sensitive sensors for measurement and instrumentation. This research aims to contribute vital research knowledge for developing sustainable four-bar dynamic testing mechanisms.

*Keywords:* - Four-bar mechanisms, Grashof Rotatability criteria, DE ASME Elliptic criteria, Accelerometer, inherent offset

Received: October 8, 2021. Revised: September 6, 2022. Accepted: October 11, 2022. Published: November 7, 2022.

## 1 Introduction

The following chapter discusses the background and motivation that played a part in the selection of this project. Moreover, it also lists the objectives and the scope of this project, along with the layout of this thesis.

### 1.1 Background

The four-bar dynamic machine is considered one of the most fundamental mechanical machines to understand the dynamics of mechanical links in a controlled system. The development of a four-bar mechanism in the form of a systematic application or being a part of any mechanical device is carried out by many industries all around the globe and studied by researchers worldwide. However,

developing a testing machine, to analyze the performance of such systems involving dynamic studies of mechanical motions, is rarely targeted.

The advancement of biomechanical engineering and the improvement in aesthetic structures usually involves the application of a four-bar mechanism, [1]. For this purpose, it becomes an ulterior requirement for the designers to test the mechanism of links for their proper functionality and implications on the machine requirement. Also, the requirement of such testing mechanisms for academic purposes is extremely important and in dire need of laboratories in the country's public, semi-governmental, and private sector institutions. The already available testing mechanisms are not only costly solutions but also apply complex single-

purpose testing procedures, as presented in the literature review.

### 1.2 Mechanism

A mechanism is a system of connected elements to achieve a predetermined pathway. It is operated under characteristic parameters which define the quantity and the quality of the machines, for instance, the load, the speed (revolution per minute, RPM), and power. An example of a mechanism is given in Figure 1.

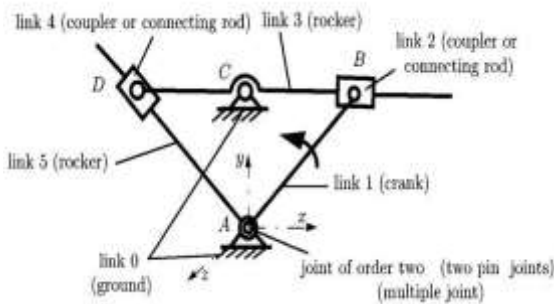


Fig. 1: An example of a mechanism [1]

#### 1.2.1 Types of Motions

A large majority of mechanisms exhibit motions in a parallel plane. It is marked by the rotation of a linkage about an axis perpendicular to the plane motion. A spatial mechanism, in contrast, allows motion (rotation and translation) in three directions Figure 2. These are imposed by the constraints of the joints (spherical, helical, cylindrical), [2]. A linkage that undergoes rotation and translation simultaneously exhibits complex motions that are hard to predict.

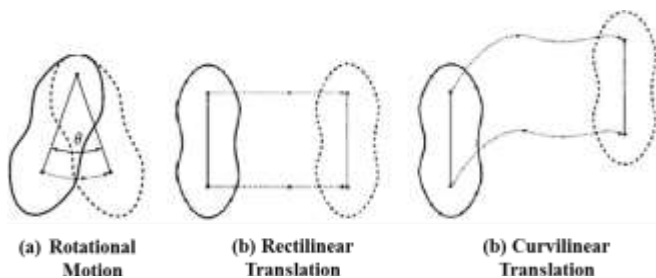


Fig. 2: Different types of motion [2]

#### 1.2.2 Four Bar Mechanisms

The simplest closed-loop mechanism having three movable links (crank, rocker, coupler) and one fixed link (ground) is called a four-bar mechanism. The link connecting to the power source is termed a crank (2), while the link associated with the output load is called the rocker (output link) (4). The coupler links the crank to the rocker. Figure 3 shows a simple four-bar.

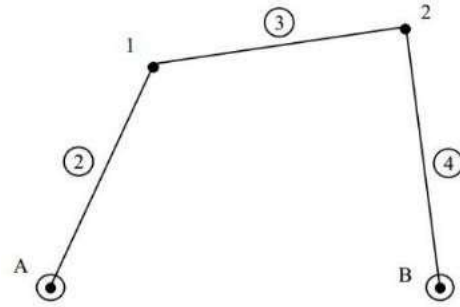


Fig. 3: A simple four-bar mechanism [2]

The four-bar mechanisms are available in various configurations for different purposes.

#### 1.2.3 Classification of Four-Bar Mechanisms

- For **Class I** four-bar  $S + L \leq P + Q$ , so based on where the shortest link is located, the 4-bar linkage is as follows:
  - Crank-crank if S is the ground link
  - Crank-rocker if S is the input link
  - Double-rocker if S is the coupler link
  - Rocker-crank if S is the output link
- For **Class II** four-bar  $S + L > P + Q$ , so triple rocker configurations of various inversions will be obtained, as shown in Figure 4.

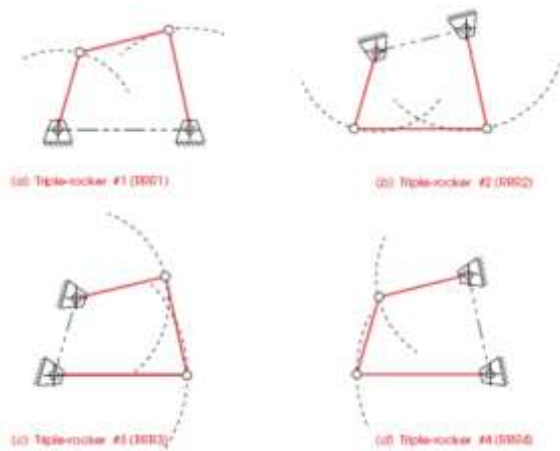


Fig. 4: Motions of class II four-bar linkages [3]

- For **Class III** four-bar  $S + L = P + Q$ , so the variations are as follows (Figure 5):

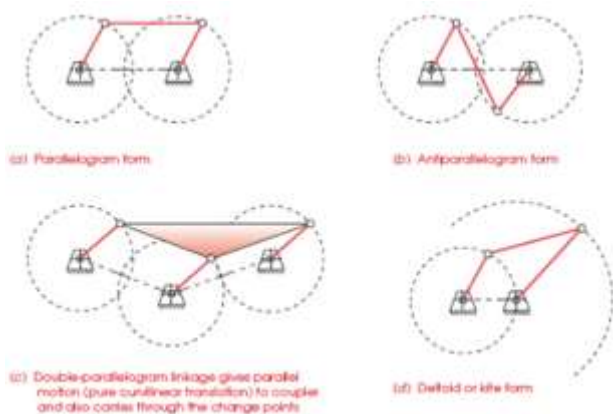


Fig. 5: Variations of class III four-bar linkages [3]

### 1.3 Degree of Freedom and Mobility

Degree of Freedom (DOF), also referred to the mobility of a motion, is a term that defines the quantity of the motion achieved by mechanisms. The number of independent coordinates used to describe the motions usually gives the degree of freedom. The greater the degree of freedom, the versatile be the motion, [4]. There is no requirement that a mechanism has only one DOF, although that is often desirable for simplicity. The DOF of any assembly of links can be predicted from an investigation of the Gruebler condition, [4].

$$M = 3L - 1 - 2J_1 - J_2 \quad (1)$$

where,

L is the number of links with the ground link

J<sub>1</sub> = Number of one degree of freedom joints full

joints J<sub>2</sub> = Number of two degrees of freedom joints half joints

The above relation has been used to determine the DOF of a closed and open four-bar mechanism in Figure 6.

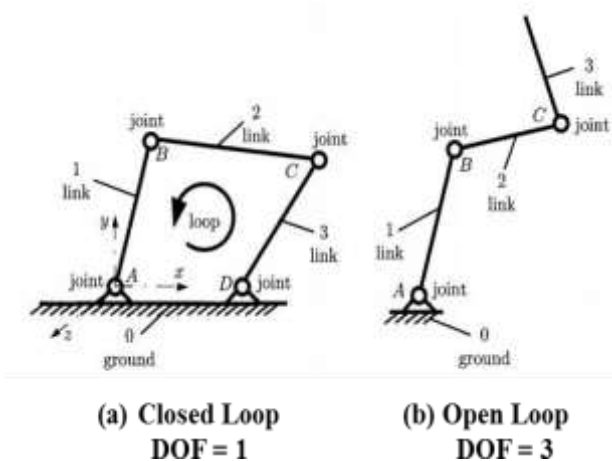


Fig. 6: DOF of a simple closed loop and open loop four-bar mechanism [4]

### 1.3.1 Rotatability Criteria

Many mechanisms include 4-bar, 6-bar, or 8-bar linkages with varied configurations. It is considered the best if a four-bar works for an application. Grashof's theorem is used to check the rotatability of the driving linkage, [5]. This condition must be satisfied for the lengths of the links for a mechanism.

Grashof's theorem states that at least one link will rotate through 360 if the following condition is met.

$$S + L < P + Q \quad (2)$$

where,

S = Shortest link,

L = Longest link,

P & Q = Other two links

If Grashof's theorem is not satisfied, no link will rotate through 360. If  $S + L > P + Q$ , the 4-bar linkage is a triple rocker.

### 1.3.2 Balancing Components in 4-Bar Mechanisms

It is a prerequisite for properly functioning mechanisms to balance all the shaking moments and the shaking forces. A mechanism can be statically or dynamically balanced. Static balance, the subset of the dynamic balance, requires only the static forces to be balanced, ignoring the moments. Rotating parts should be designed to be inherently balanced by their geometry, [6]. However, the vagaries of production tolerances guarantee that there will still be some small unbalance in each part. Thus, a mechanism must be dynamically balanced. For the dynamic balance of the four-bar mechanisms, counterweights are introduced at the crank and the rocker.

### 1.3.3 Counterweights

Counterweights are designed using the force and the mass balance in the four bars. Note that the process of statically balancing a rotating link, in effect, forces its mass center (CG) to be at its fixed pivot and thus be stationary. A coupler has no fixed pivot; thus, its mass center is generally always in motion. No matter its complexity, any mechanism will have a single overall global mass center located at some point for every instantaneous position, [7]. The use of a counterweight to balance a mechanism is shown in Figure 7.

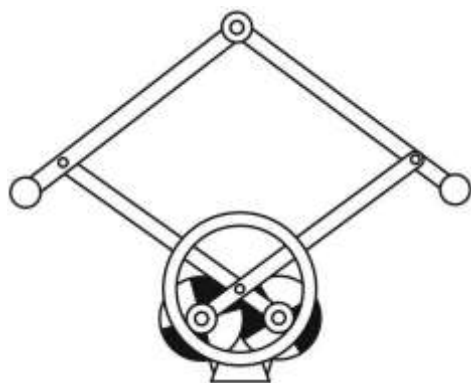


Fig. 7: Mechanism balanced by a counterweight [7]

The total mass of the system is simply the sum of the individual link masses:

$$m_t = m_1 + m_2 + m_3 \quad (3)$$

The total mass moment of the origin must be equal to the sum of the mass moments due to the individual links, [10].

$$\sum Mo_2 = m_t R_t = m_2 R_2 + m_3 R_3 + m_4 R_4 \quad (4)$$

The mathematical and trigonometrical functions are performed for relations for R2, R3, and R4 are found.

### 1.3.4 Analysis of Four-Bar Mechanisms

The analysis is performed on the mechanism, especially the coupler link, to find the velocity and acceleration values at various locations, which would help determine the critical points on the coupler. Figure 8 shows the analysis of a simple four-bar mechanism.

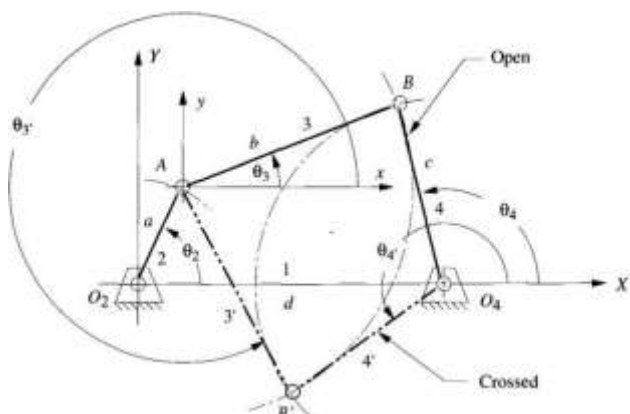


Fig. 8: Analysis of a four-bar mechanism [8]

The two types of analysis include:

- Velocity Analysis
- Acceleration Analysis

### 1.3.5 Velocity Analysis

Velocity is important because it affects the time required to perform a given operation, such as the machining of a part. Power is the product of force, linear velocity, torque, and angular velocity. For the transmission of a given amount of power, the forces, and stresses in the various links of a mechanism can be reduced by altering the velocities through a change in the size of the links. Friction and wear on machine parts also depend upon velocity, [9]. Velocity analysis can be done by using:

- Graphical Positioning Method
- Relative Velocity Method

### 1.3.6 Acceleration Analysis

Acceleration analysis is important if a dynamic force analysis is to be performed. Acceleration in linkages is important because inertia forces are proportional to rectilinear acceleration and inertia torques are proportional to angular accelerations. Inertia forces influence stresses in the parts of the machine, the bearing loads, vibration, and noise. Moreover, acceleration analysis of a mechanism is done by adding relative accelerations. This method is like the velocity method that uses relative velocities, [8]. Calculating the acceleration vector involves relative analysis, which is then verified by the position analysis of the linkages.

### 1.3.7 Dynamic Force Analysis

It is necessary to design a mechanism to know how forces are transmitted from the input to the output so that the components of the mechanism can be properly sized to withstand the stresses induced. Thus, the dynamic force analysis (shown in Figure 9) plays a key role in determining the forces acting on the linkages.

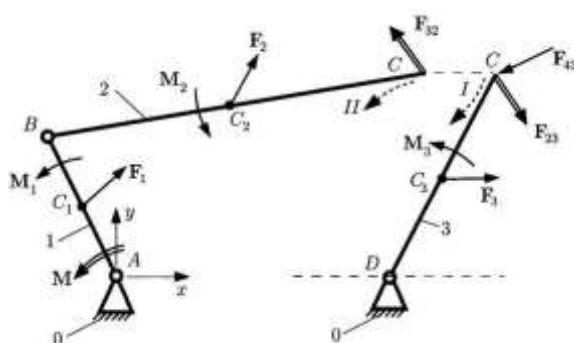


Fig. 9: Force analysis of a four-bar mechanism [9]

## 2 Literature Review

This chapter describes the various applications of the four-bar mechanisms and the rationale for this study aimed to develop after this study.

The regulation of the crank angular speed of the four-bar mechanism is considered one of the most important and tricky tasks, which is mostly dependent upon the application. It is also a matter of common observation that the angular velocity of the crank is assumed to be constant in mechanism analysis. However, this assumption fails when the electric motor is used to drive the mechanism. Furthermore, it has been assessed that the Fuzzy Logic Controller performs efficiently compared to the PID counterpart, [10]. To analyze crank angular speed fluctuations, research is performed to develop a state space mathematical model for such an electric motor-driven system, [11]. This model is then controlled with a fuzzy logic controller and compared with a PID controller. The obtained results prove that the speed fluctuations and rise-time overshoot percentage are very much controlled with the help of fuzzy logic controller compared to a PID controller, [11]. The schematic of a four-bar mechanism is presented in Figure 10.

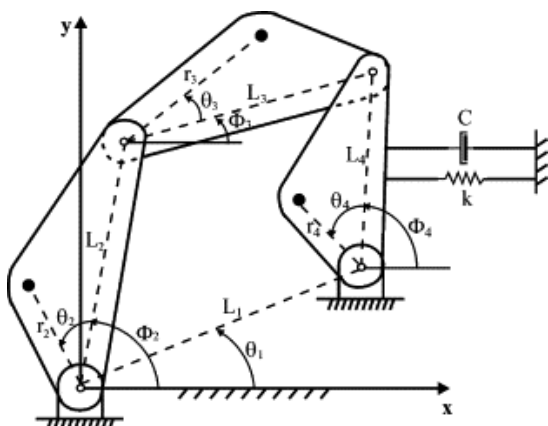


Fig. 10: Schematic of a four-bar mechanism [11]

An important consideration in this regard is the inclusion of clearance in the analysis of four bar mechanisms. A simple mechanism is developed by adding a single spring between the journal and the sleeve. The simulations and experimental tests performed on this mechanism using the platforms of ADAMS and MATLAB proved that the dynamic behavior of the mechanism was much improved due to the continuous contact between the sleeve and the journal, [12]. It is also analyzed with the help of experiments that the torque is also increased after the implication of spring in the designed model. Overall, only optimization is necessary to investigate the best parameters of the spring to

reduce the clearance effect as much as possible, [13]. The experimental setup for clearance calculation of Vector R is presented in Figure 11.

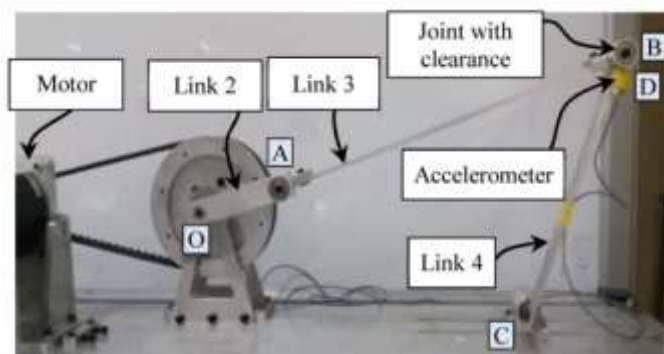


Fig. 11: Experimental Setup for clearance calculation of Vector R [12]

Another important factor in this regard is the control AC motor-driven four-bar mechanism with the help of Continuous Variable Transmission (CVT). It is a matter of fact that different applications require different speeds and manufacturing attributes in a four-bar mechanism. Therefore, continuously variable transmission is considered the miracle of modern times because it allows the motor to run at its nominal point in all conditions, [14]. Therefore, the increase in efficiency can also be observed along with the fulfillment of the application of variable transmission. Hence, a theoretical model is developed, and the Simulations are performed on the four-bar mechanism with and without the continuous variable transmission so the comparison can be analyzed. This comparison proved that continuously variable transmission is a more feasible solution for the designated applications of the four-bar mechanism, [14]. The reduction in noise due to the use of CVT is presented in Figure 12.

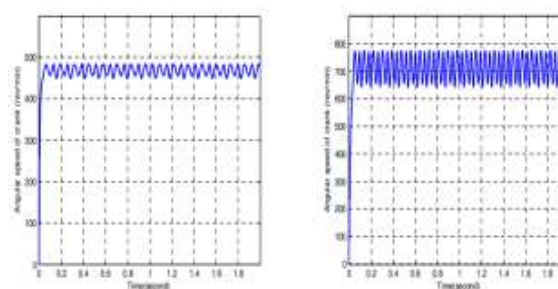


Fig. 12: Reduction in noise due to the use of CVT [14]

The research on exoskeleton robotics has been observed to have a good pace in modern times. Technological advancement is expected to meet the recent need for a workforce in the industry, [15].

Therefore, research is also performed on different combinations of active and passive actuators based on four-bar mechanisms to replicate the different positions of the actual work. After repetitive simulation checks, a combination with a linear spring based on four bar mechanism and a rotary actuator is proposed, verifying experimentally, [15].

The four-bar mechanism in exoskeleton structure is presented in Figure 13.

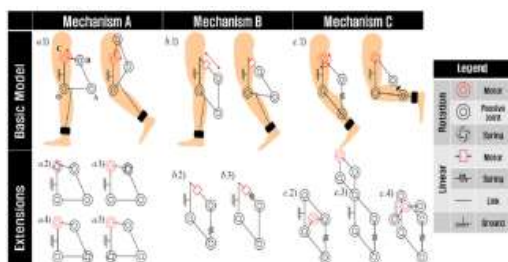


Fig. 13: Four-Bar mechanism in exoskeleton structure, [15]

Biomechanical systems are mostly defined by the system's functional property and underlying morphology. Different four-bar mechanisms are used in the biomechanical structures because they are used to convert the expected functional performance into morphological development, [16]. The three-dimensional complex motion of different insects and birds are tried to be replicated in the form of micro air vehicles with flapping wings which offer quite some challenge because of the availability of limited design variables, [17]. The wing motions of these birds and insects that enable them to hover, fly, and undertake random complex motions result from unique patterns due to favorable aerodynamic forces. The wing's spatial flapping motion can be considered a viable solution with the help of a four-bar flapping mechanism, as it is a lightweight design. However, testing this flapping mechanism is considered a challenge that needs to be addressed, [17]. The spherical four-bar mechanism for flapping in micro-air vehicle is presented in Figure 14.



Fig. 14: Spherical Four-bar Mechanism for flapping in Micro-air vehicle [17]

The actuation based upon the cable-driven mechanism is considered a less efficient design due to inaccuracy in the range of motion and weak structural durability. The researcher used a trans-radial prosthesis based upon a four-bar linkage mechanism to improve structural efficiency, [18]. This prosthesis is a wearable device that helps replace the missing anatomical segment under the elbow. Many structural problems, less ergonomic design issues, and related problems were still observed in this system. A proper testing mechanism, not only for the design but also for the dynamic performance, can be considered an important need here because only the static analysis simulation was used to test the durability, and the motion capture analysis was used to test the dynamic properties, [18].

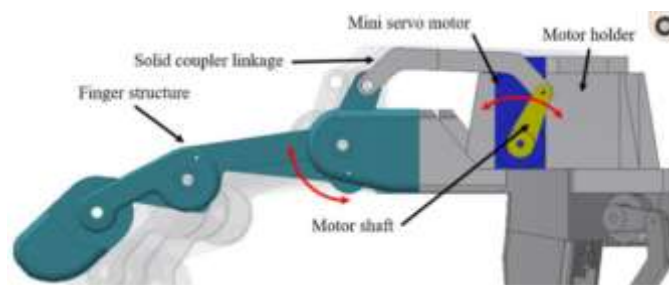


Fig. 15: Robotic hand testing [18]

The planar four-bar mechanism has numerous daily-life applications, including car wipers, door frames, bicycles, etc. It is also called as 4R mechanism because it usually consists of four revolute parts. Due to this geometry, this four-bar mechanism is the smallest and simplest closed-chain moveable linkage, [19]. The numerical computation for a planar four-bar mechanism in the configuration of the crank rocker is performed using MATLAB. The kinematic analysis of the mechanism is undertaken after mathematical modeling through Euler's equation and Newton's second law. RecurDyn is also used to compare and validate the results achieved with the help of multibody dynamic analysis, [20]. The robotic hand testing is presented in Figure 15.

## 2.1 Rationale of Research

The complete analysis of published research articles and contributions is made to attain knowledge of existing mechanisms and machines discussed or developed for testing different combinations of four-bar mechanisms. The secondary search, the most relevant part of which is explained in the complete literature review, put forward some very good and effective solutions for testing different four-bar mechanisms that can be used for specific

applications. Although sound research has been made by different researchers all around the globe in analyzing different four-bar mechanisms and applications with or without clearances, a scientific research gap can be detected in developing a universal 4-bar testing machine that can be used for the testing of different four power mechanisms meeting the Grashoff's rotatability criteria.

The detailed analysis of the literature, discussed in the above section, vividly generates the need for research in the section of testing the four-bar mechanisms with the help of active testing mechanism to effectively generate a need-based or customized design for the four-bar mechanism assessing the design variables using multiple iterations to look for most appropriate real-time dimensional constraints or design ranges.

### 3 Design Methodology

This chapter deals with the approach to designing the four-bar mechanism and the criteria for selecting the belt and pulley, bearings, and motor. Moreover, it includes the CAD models of the individual linkages and components and the final assembly of the mechanism.

#### 3.1 Linkage Design

One degree of freedom (DOF) planar mechanism was considered for designing the four-bar linkages, with the total number of links equaling four. All the links were assumed to be binary for the simplicity of the design and the crank-rocker inversion, along with Barker's classification of planar four-bar linkages, was used. The inversion used for the linkage was L2 = S = Input Link of Class 1-2 and Grashof crank-rocker-rocker (GCRR) according to Barker designation, [21].

##### 3.1.1 Two-Position Synthesis

The graphical method was used as it is the simplest procedure. The two-position synthesis has two categories, which include (i) Rocker Output and (ii) Coupler Output. Rocker output is suitable for Grashof crank rockers. It is a case of function generation in which two discrete angular positions are given as output functions, [21]. This approach (as shown in Figure 16) is to perform the position analysis of the four-bar mechanism.

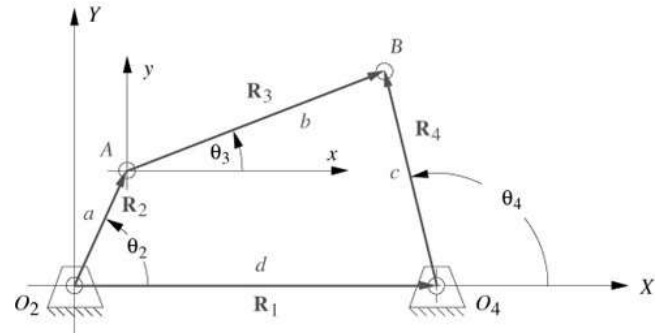


Fig. 16: Position analysis of four-bar linkage [21]

Table 1 summarizes the dimensions and mass properties of the linkages used in the four-bar mechanism.

Table 1. Properties of different links

Link	Crank	Coupler	Rocker
Lengths (mm)	110	310	220
Thickness (mm)	10	15	10
Mass (kg)	0.39	1.19	0.52
Moment of Inertia (Iz)/kg.mm <sup>2</sup>	652.5	14500	3590
Distance of COG from joint, r (mm)	50	160	110

##### 3.1.2 Rotatability Criteria Assessment

The rotatability criteria for the linkage was tested using the Grashof condition, for which the following relation were checked, [22]:

$$S + L < P + Q \quad (5)$$

S= shortest length,  
 L=longest length,  
 P and Q are the other two lengths.

It was found that the Grashof condition was satisfied as the relation held. Therefore, the link lengths mentioned in the table above were then used for the design of the linkage to get possible output motion. The CAD Model of linkages is shown in Figure 17, Figure 18, Figure 19, Figure 20, and Figure 21.

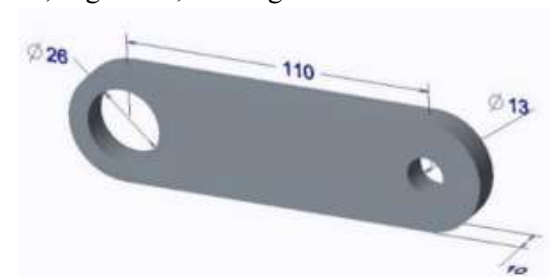


Fig. 17: Crank

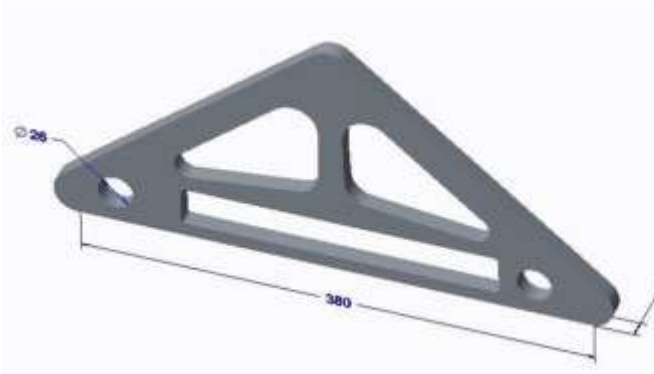


Fig. 18: Coupler

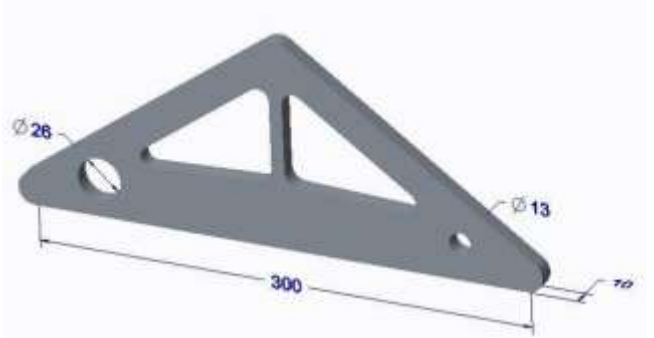


Fig. 19: Rocker

### 3.2 Counterweights Design

Due to the rotation and cyclic motion of linkages, shaking forces and torques are induced at the ground pivots. To reduce this unbalance, counterweights are designed. As stated in the previous chapter, counterweights are designed using the force and the mass balance in the four-bar (using Eq. 6 and Eq. 7) for designing the counterweights for the crank and rocker, respectively, [23].

$$m_2 b_2 e^{i\theta} = m_3 \left( b_3 \cdot \frac{l_3}{l_2} \cdot e^{i\theta} - l_2 \right) \quad (6)$$

$$m_4 b_4 e^{i\theta} = -m_3 b_3 \cdot \frac{l_4}{l_3} \cdot e^{i\theta} \quad (7)$$

Using the relations stated earlier, the CAD models of the designed counterweights (both for the crank and rocker) are shown below:

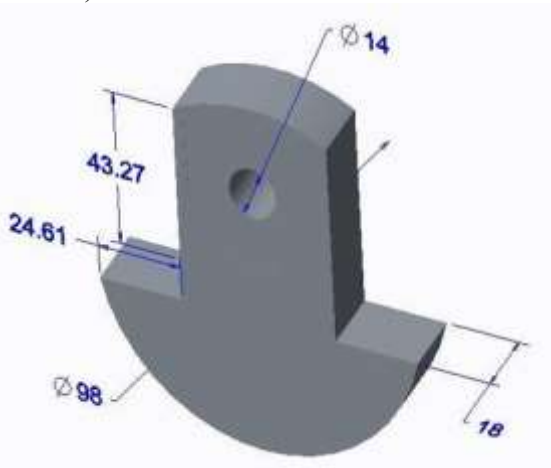


Fig. 20: Counterweight for crank

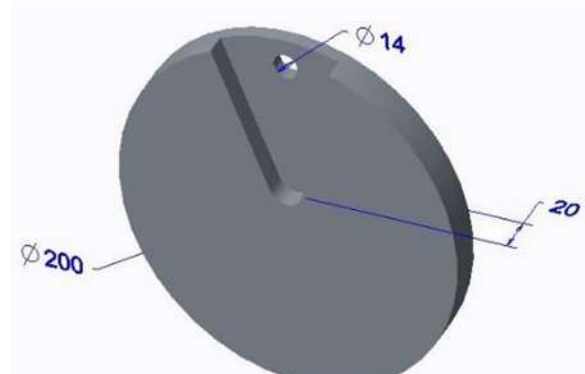


Fig. 21: Counterweight for rocker

Table 2 summarizes the dimensions and mass properties of both counterweights.

Table 2. Properties of counterweights

Link	Counterweight-Crank	Counterweight-Rocker
Diameter (mm)	45.72	68.8
Thickness (mm)	23.00	18.50
Mass (kg)	1.96	2.64
Distance of CG from Pivot, r (mm)	45.72	68.8

### 3.3 Flywheel Design

The flywheel was designed to store kinetic energy and keep the torque fluctuations required to drive the linkage to a minimum. The previous chapter used the following relations following the energy method to design the flywheel, [24].

$$E = \frac{1}{2} I \omega^2 \quad (8)$$

$$T = I \alpha \quad (9)$$

$$\int_{\theta @ \omega_{Min}}^{\theta @ \omega_{Max}} (T_L - T_{avg}) d\theta = \frac{1}{2} I (\omega_{Max}^2 - \omega_{Min}^2) \quad (10)$$

The left side of this equation represents a change in energy between the shaft's maximum and minimum angular velocities. It is integrated to obtain the area under the torque diagram, illustrated in Figure 22. The figure shows the torque variations in the T12, which is the torque applied by the crank over its one complete revolution.

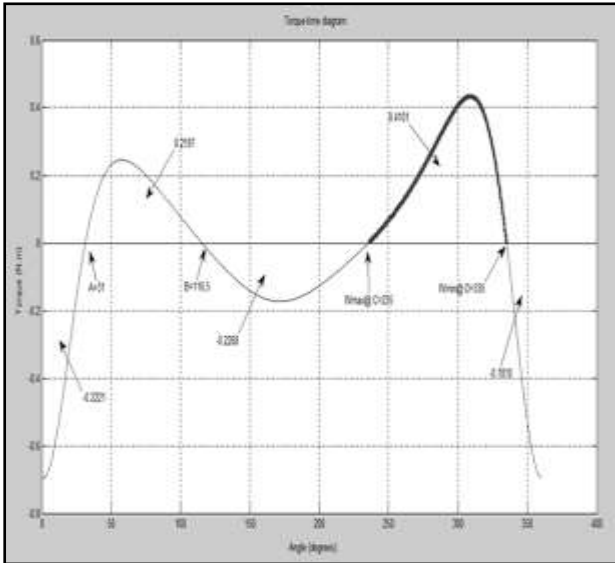


Fig. 22: Torque-time diagram for T12

Numerical Integration of the torque-time diagram from crossover to crossover is done to calculate the area under the curve for all intervals. These areas are used to evaluate the accumulated sum. These show accumulation of energy after each interval. As shown in Table 3, the value where the sum is minimum gives a point of maximum angular velocity, and the value where the sum is maximum gives a point of minimum angular velocity.

The area under the thick curve in Figure 22 gives the total amount of energy to be stored by the flywheel, shown in Table 3.

Table 3. Area values calculated from Figure 22

	Area (N.m.rad)	Accumulated Sum
A-B	0.2197	0.2197
B-C	-0.2268	-0.007 $\omega_{max}$ @ C
C-D	0.4101	0.403 $\omega_{min}$ @ D
Remaining area	-0.403	$6.28 \times 10^{-5}$

Therefore,

$$\text{Total change in energy} = \Delta E = E @ \omega_{Max} - E @ \omega_{Min} = 0.4101 \text{ N.m.rad}$$

$$\text{Coefficient of fluctuation} = k = 5\% = 0.05$$

Flywheel is designed at an average crank angular speed of  $\omega_{avg} = 60 \text{ rpm} = 6.283 \text{ rad/s}$ .

The inertia of the flywheel was calculated using Eq. 11, as shown below:

$$I_s = \frac{E}{k \omega_{avg}^2} \quad (11)$$

$$\frac{1}{2} m r^2 = 0.207 \text{ kgm}^2 \quad (12)$$

The flywheel was designed as a disc, with Figure 23 depicting its CAD model.

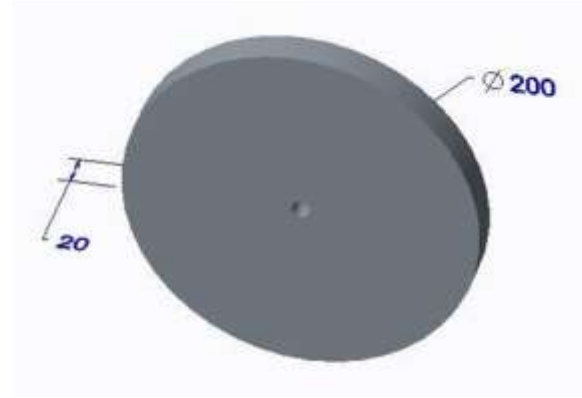


Fig. 23: Flywheel

The values of mass and diameter of the flywheel are decided after various iterations. Table 4 lists the final dimensions of the flywheel along with its mass.

Table 4: Flywheel parameters

Parameter Description	Value
Diameter (mm)	250
Thickness (mm)	17.5
Mass (kg)	6.72

### 3.4 Shaft Design

The shaft is the key component that connects the machine to the ground. The crank, rocker, and flywheel are mounted on the shafts. The motor rotates the shaft, and in turn, the crank rotates. Considering the stresses induced in the shaft, the shaft diameter is calculated using the DE-ASME Elliptic criterion, [25].

$$d = \left[ \frac{16n}{\pi} \left\{ \frac{1}{s_e} \sqrt{4(k_f M_a)^2 + \frac{1}{s_y} \sqrt{3(K_{fs} T_m)^2}} \right\} \right]^{\frac{1}{3}} \quad (13)$$

The different parameters used for shaft design are listed in Table 5.

Table 5. Parameters for shaft design

Parameters	Values
$K_f = K_t$	1.70
$K_{fs} = K_{ts}$	1.50
$K_a$	0.88
$K_b$	0.90
$K_c = K_d = K_e$	1.00
$M_a$ (N.m)	7.50
$T_m$ (N.m)	10.0
$S_{ut}$ (Pa)	$4.00 \times 10^8$
$S_e$ (Pa)	$1.59 \times 10^8$

a	2.70
b	-0.27
n	2.00
Diameter (mm)	13.7

A conservative approach selected a shaft with a diameter of 15 mm.

### 3.5 Belt and Pulley Design

A 60 Watts AC geared motor running at a maximum of 80 rpm is used to drive the shaft attached to the crank of the mechanism. The available pulley had sheave diameters of 71.1 mm for both the driven shaft and drive motor. An A30 V belt was used for the transmission of power. The service factor was chosen to be 1.3 since the application has non-uniform torque and light shock.

The following relations, Eq. 12 and Eq. 13, are used in the design and analysis of the belt and pulley, [26].

$$V = \frac{\pi dn}{12} \quad (14)$$

$$\Delta F = 63025 * \frac{H_d / N_b}{n(\frac{d}{2})} \quad (15)$$

Here, V represents the peripheral speed calculated as the angular velocity of the motor. The center-to-center distance for the pulleys to be installed is calculated from the relation above. Also, the relations between actual power and nominal power are given. These relations are then used to predict the factor of safety and the operating life in hours as given below:

$$n_{fs} = \frac{H_a N_b}{H_{nom} K_s} \quad (16)$$

$$N_p = \left[ \left( \frac{K}{T_1} \right)^{-b} + \left( \frac{K}{T_2} \right)^{-b} \right] \text{passes in } t = \frac{N_p L_p}{720V} \text{ hours} \quad (17)$$

The selected A30 belt had a safe design since the life and the safety factor were well in the prescribed range, as shown in Table 6.

Table 6. Belt specifications

Parameter	Value
Pitch length (mm)	808
Design Power, Hd (W)	123
$\Delta F$ (N)	260
Number of Passes	$6 \times 10^9$
Life (Hours)	32,800
Factor of Safety	2.88

Figure 24 shows the CAD model for pulleys and the V belt used.

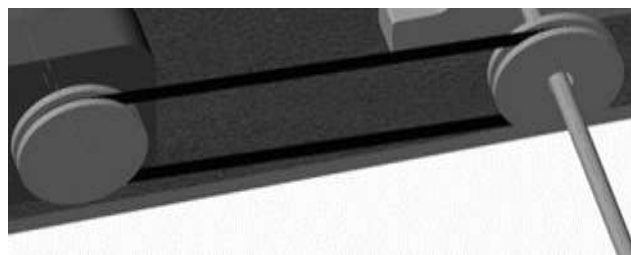


Fig. 24: Belt and pulleys

### 3.6 Motor Selection

The motor selection was based on the load requirements, angular velocity (rpm), and the torque used in the apparatus. The torque used in this formula to calculate the power required for the selected motor is the T12, which is obtained in the above section with the help of a graphical solution obtained from MATLAB while solving the theoretical kinematic model. The angular velocity is obtained from the area under the curve in the same graph, and both these values are used to calculate the power. The power selected is 60 watts, and the value is selected because it is approximately similar and very close to the theoretical power consumption assumption obtained from the theoretical assessment mentioned in the earlier portion of the theoretical kinematic analysis. A geared motor had to be employed to reduce the speed manifold since the required speed was lower than conventional motors. A parallel head shaft with single-phase AC input was available in the motor, [27]. The required torque and the rpm gave the power specification as shown below.

$$Power = T\omega = \frac{3.8 \times (140 \times 2\pi)}{60} = 55 \text{ Watts}$$

The motor specification is listed in Table 7.

Table 7. Motor specification

Parameter	Value
Output Power (W)	60
Voltage (VAC)	Single-Phase 110/115 VAC
Frame Size (mm)	90
Current (A)	1.21
Gear Ratio	18:01
Rated Speed (rpm)	80
Rated Torque (N.m)	5.80
Output Shaft Diameter (mm)	19.05

### 3.7 Bearing Design

As stated in the previous chapter, the forces acting at the pin joints of the linkage were needed to calculate the bearing diameter. The selection for bearing was done mainly for radial loads acting in a plane of motion, as thrust loads were negligible. For variable loading, [28],

$$F_{eq} = \left[ \frac{1}{\phi} \int_0^{\phi} F^a d\theta \right]^{1/a} \quad (18)$$

From reaction forces acting on joints,  $Fd = 5.5 N$ . The C10 catalog entry is found using following equation (Eq. 19)

$$C = 0.25 \left\{ \left[ l_p - \frac{\pi}{2}(D + d) \right] + \sqrt{\left[ l_p - \frac{\pi}{2}(D + d) \right]^2 - 2(D + d)^2} \right\} \quad (19)$$

By putting  $a = 3$ , other parameters are listed in Table 8

Table 8. Parameters for bearing selection

Application Factor, af	1.2
Revolutions per Minute (rpm)	60
Bearing Life, LD (hours)	5000
Revolutions for Rating Life, L10	106
Reliability factor, RD	0.99
Typical Weibull Parameters	
x0	0.02
$\theta$	4.459
b	1.483

It gives  $C10 = 28.5 N$ .

After bearing design and analysis, the bearing is selected from the manufacturer's catalog according to the required bore diameter and life calculated.

### 3.8 Dynamic Analysis

To get an insight into the functional behavior of the four-bar mechanism, the determination of displacement and velocity at the required location of the coupler link was required. Therefore, the kinematic analysis needed to be performed to determine the center of gravity and angular velocities at different locations of the coupler link. Link lengths, mass values, and other parameters were used to determine the forces applied by or on the linkages, [29]. The applied torques were predefined at all points of interest to solve for the pin forces.

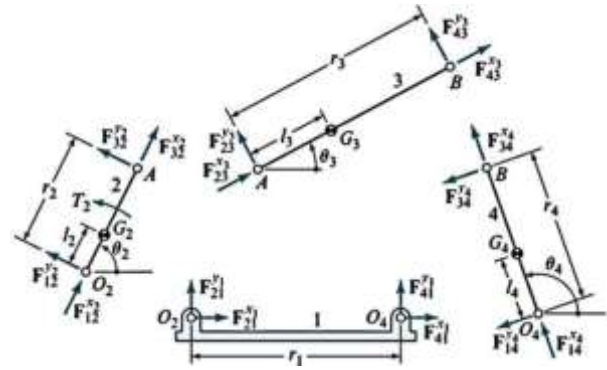


Fig. 25: Nomenclature of dynamic parameters of a four-bar mechanism [29]

The dynamic parameters and force locations were defined concerning a local, moving but non-rotating axis. For each linkage, two forces and torque were unknown entities. This meant nine equations with nine unknowns would be obtained. Therefore, a  $9 \times 9$  matrix representing the forces being applied on all 3 linkages (using the nomenclature of Figure 25) is shown in Eq. 20 below.

$$\begin{bmatrix}
 1 & 0 & 1 & 0 & 0 & 0 & 0 & 0 & 0 \\
 0 & 1 & 0 & 1 & 0 & 0 & 0 & 0 & 0 \\
 -R_{12y} & R_{12x} & -R_{32y} & R_{32x} & 0 & 0 & 0 & 0 & 1 \\
 0 & 0 & -1 & 0 & 1 & 0 & 0 & 0 & 0 \\
 0 & 0 & 0 & -1 & 0 & 1 & 0 & 0 & 0 \\
 0 & 0 & R_{23y} & -R_{23x} & -R_{43y} & R_{43x} & 0 & 0 & 0 \\
 0 & 0 & 0 & 0 & -1 & 0 & 1 & 0 & 0 \\
 0 & 0 & 0 & 0 & 0 & -1 & 0 & 1 & 0 \\
 0 & 0 & 0 & 0 & R_{34y} & -R_{34x} & -R_{14y} & R_{14x} & 0
 \end{bmatrix}
 \times
 \begin{bmatrix}
 F_{12x} \\
 F_{12y} \\
 F_{32x} \\
 F_{32y} \\
 F_{43x} \\
 F_{43y} \\
 F_{14x} \\
 F_{14y} \\
 T_{12}
 \end{bmatrix}
 =
 \begin{bmatrix}
 m_2 a_{G2x} \\
 m_2 a_{G2y} \\
 I_{G2} \alpha_2 \\
 m_3 a_{G3x} - F_{px} \\
 m_3 a_{G3y} - F_{py} \\
 I_{G3} \alpha_3 - R_{px} F_{py} + R_{py} F_{px} \\
 m_4 a_{G4x} \\
 m_4 a_{G4y} \\
 I_{G4} \alpha_4 - T_4
 \end{bmatrix} \quad (20)$$

These kinematic parameters were then substituted in the matrix, and the matrix was solved using a numerical solver, and the plots of forces and torques were obtained. Figure 26 presents the graph of torque applied on the crank vs crank angle.

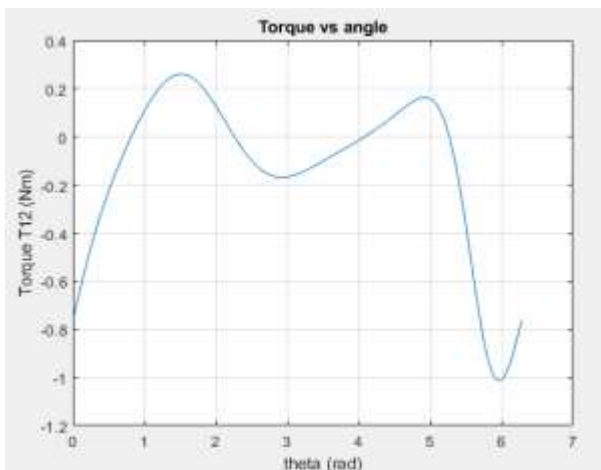


Fig. 26: Graph of torque applied on the crank vs crank angle

The maximum torque applied on the crank was 0.28 Nm at a crank angle of 86°, with the minimum torque value being -1.02 Nm at a crank angle of 342°. Figure 27 and Figure 28 show the variation of the force being applied on the crank joints by the rocker and coupler against the crank angle, respectively.

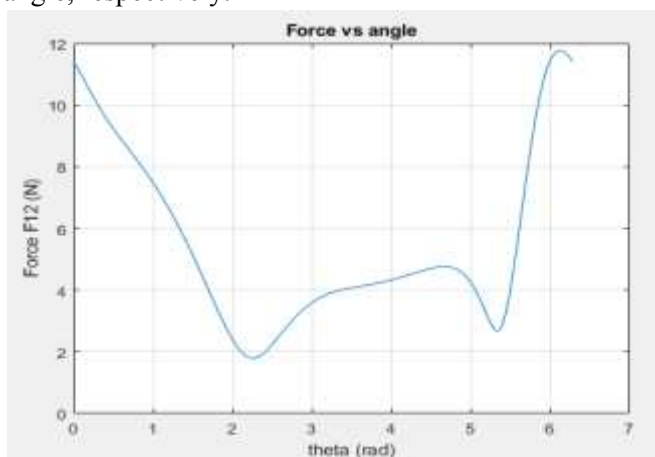


Fig. 27: Graph of force applied on crank by ground vs crank angle

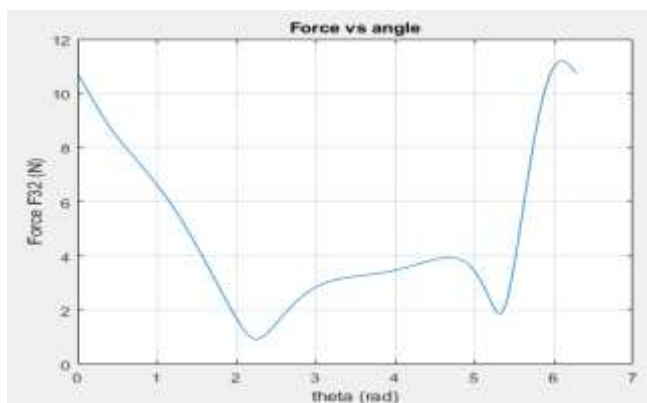


Fig. 28: Graph of force applied on crank by coupler vs crank angle

It can be seen that both follow same trend in force variation against the crank angle. For Figure 27, the maximum value of force applied by ground is 11.95 N on the crank at crank angle of 345°, with the minimum value of force applied being 1.95 N at crank angle of 135°. For Figure 28, the maximum value of force applied by coupler is 11.4 N on the crank at crank angle of 345°, with the minimum value of force applied being 1.05 N at crank angle of 142°. Figure 29 and Figure 30 illustrate the force being applied by rocker on coupler and the force being applied by ground on rocker against the crank angle.

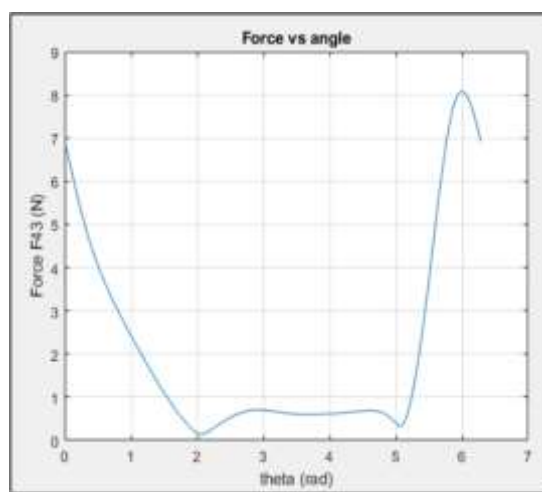


Fig. 29: Graph of force applied on coupler by rocker vs crank angle

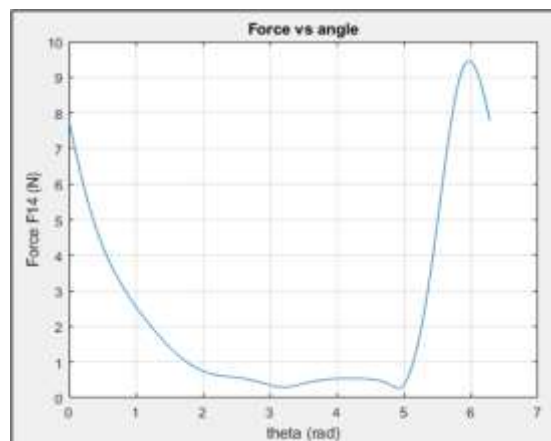


Fig. 30: Graph of force applied on rocker by ground vs crank angle

It can be seen that a similar trend in force variation against the crank angle is followed. For Figure 29, the maximum value of force applied by the rocker is 8.07 N on the coupler at a crank angle of 343°, with the minimum value of force applied being 0.16 N at a crank angle of 120°. For Figure 30, the maximum value of force applied by ground is 9.42 N on the

rocker at a crank angle of  $338^\circ$ , with the minimum value of force applied being 0.23 N at a crank angle of  $285^\circ$ . The final assembly of the cad model is presented in Figure 31.

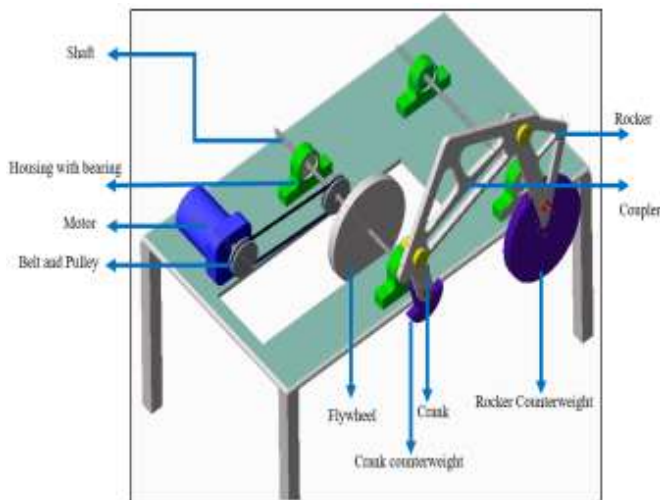


Fig. 31: Final assembly of the cad model

## 4 Prototype Development

This chapter deals with the techniques adopted and the procedures followed for the fabrication of the mechanism.

### 4.1 Materials Selection

Material choice is a crucial prerequisite for the design as well as for the budget analysis. The material selection was done by considering the economical aspect and the strength required for the design, [30].

#### 4.1.1 Linkages

The linkages were to be mounted on a shaft and driven by an electric motor. Thus, it needed to be lightweight and easily moved at greater speeds. Heavier materials would require a motor of high-power requirements that would be expensive and not easy to mount, [21]. Aluminum 6061 was considered lighter in weight and relatively easier for the machine. The thicknesses were also under a unit cm to avoid disruptions, but they were not kept too small because joints connecting the two linkages required certain mass support.

#### 4.1.2 Counterweights

The crank and the counterweights were made of mild steel because of the requirement for heavier-density material. Moreover, the crank was responsible for the transmission of power from the motor to the entire mechanism due to which great strengths were required at its disposal.

Counterweights used to balance the mechanism were made of mild steel for greater endurance.

#### 4.1.3 Shafts

The material used during the design was mild steel. Its ability to resist bending loads, torsional loads and transverse shear loading made it a preferred choice for material for shafts.

## 4.2 Manufacturing of Linkages

After the purchase of materials such as aluminum plates and discs of mild steel, the manufacturing of linkages was pursued. First of all, the triangular shapes of links were traced on the plates of aluminum and mild steel, then using the horizontal milling machine (Figure 32), cut these shapes.



Fig. 32: Cutting of coupler on horizontal milling machine

Figure 33 depicts the linkage obtained after it was machined using the milling machine.



Fig. 33: Coupler link after cutting

#### 4.2.1 Material Removal

After cutting out the triangular metal pieces, internal slots had to be made in the linkages for weight reduction as the required mass of the linkages was achieved. Therefore, several holes were made through the marked slots by drilling as shown in Figure 34. Then vertical milling machine was used

to make multiple passes for complete material removal required to make slots in the linkages.



Fig. 34: Machining of the coupler

Figure 35 and Figure 36 depict final linkages obtained after finishing.



Fig. 35: Fabricated linkages (coupler)



Fig. 36: Fabricated linkages (rocker)

### 4.3 Fabrication of Auxiliary Components

In addition to the linkages of the four-bar mechanism, the fabrication of other components e.g., balancing counterweights, shafts, pin joint, and base frame, was performed. Several manufacturing processes, including lathing on the shaft and stud and welding on the frame, were undertaken and the components obtained after these operations had been used. The pin joint/stud is presented in Figure 37. Similarly, the bearing with holder bolted to frame is presented in Figure 38.



Fig. 37: Pin joint/stud Figure



Fig. 38: Bearing with holder bolted to frame

### 4.4 Assembly

After the fabrication of the components was completed, the mechanism assembly was started. During this process, the shaft assembly was a crucial step, as even slight inaccuracy in the alignment of the shafts made the results obtained from the analysis invalid. Therefore, special care was adopted while the shaft assembly was being done to ensure that they were perfectly aligned, parallel to each other, for maximum power transmission and smooth movement of the assembly. The shaft assembly is presented in Figure 39. Similarly, the crank and counterweight are presented in Figure 40.



Fig. 39: Shaft assembly



Fig. 40: Crank and counterweight

The shaft and bearing holder assembly shown in the figure holds key importance since the distance between two sets of shafts decides the length of the ground link prescribed in the design process. The rocker and the crank were made rigid with the shaft by locking them with a key. Also, the components responsible for power transmission was assembled, i.e., the pulley was seated on the shaft and fixed with a screw.

#### 4.4.1 Belt and Pulley

Once the pulley was fixed on the motor shafts and crank, the crankshaft was loosened to position the belt on the sheave. The shaft was then tightened to ensure tension in the pulley. The greater the tension more efficient will be the power transmission. Figure 41 shows the final assembly obtained for the belt and pulley.

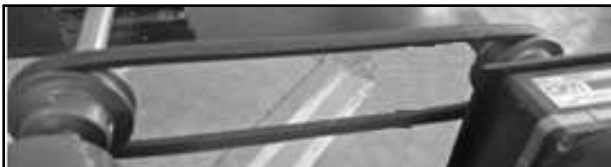


Fig. 41: Assembly of belt & pulley

#### 4.4.2 Motor Assembly

The assembly of the motor was a crucial part of the process, as the alignment of the motor with the driven shaft and pulley plays a significant role in power transmission. The motor was fixed on the base frame by a holding plate welded to the frame. A potentiometer was attached, which could vary the voltage supplied to the motor, thus controlling its rpm. The assembly of the motor is shown in Figure 42.



Fig. 42: Motor with potentiometer

#### 4.4.3 Mounting of Electronic Components

The rotary encoder was fixed with the crankshaft such that the shaft and the knob of the encoder rotated together while the encoder was grounded on the frame. Similarly, the rotary potentiometer was attached to the rocker shaft. The accelerometer was fixed on a coupler point to give values in all directions. Arduino UNO and circuit boards were placed on the base frame.

#### 4.5 Assembled Apparatus

Figure 43 shows the apparatus after performing the assembly:

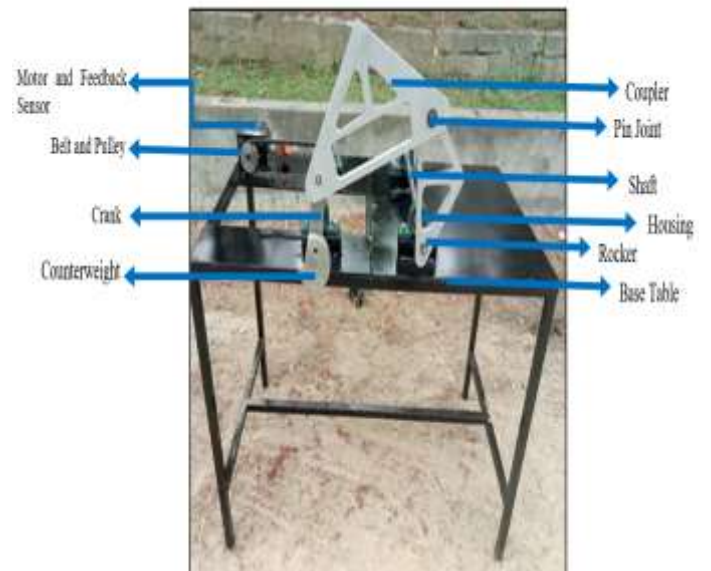


Fig. 43: Final assembly of the mechanism

### 5 Program Testing and Findings

This chapter includes the trial runs and tests performed on the written code to obtain the required acceleration, velocity, and displacement plots.

### 5.1 Theoretical Analysis using MATLAB

The sinusoidal variations of acceleration, velocity, and displacement plots are shown. The graphs are obtained with the help of kinematic analysis on software. The code is written in Matlab (provided in the appendix to have the theoretical acceleration curve of the coupler joint with the help of a four-bar kinematic equation, as given in Eq. 20. The coupler point- acceleration vs time is presented in Figure 44.

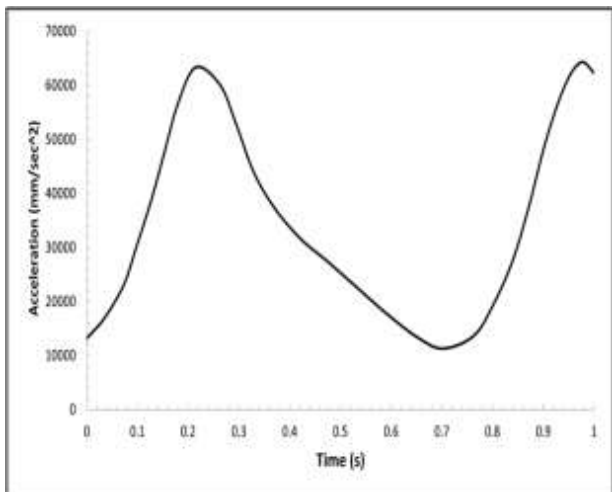


Fig. 44: Coupler point- acceleration vs time

The maximum acceleration value obtained from the software is about 63422 mm/s<sup>2</sup>. The trend is much smoother than the plot obtained by analysis of a real small-scale model, which will be shown in the next section. This is because noise and external vibrational effects are not included in the simulation, and only the formula is used to calculate the acceleration of the coupler point.

The integration of the acceleration curve with the help of data points in Matlab provided the velocity curve of the coupler point. The coupler point- velocity vs time is presented in Figure 45.

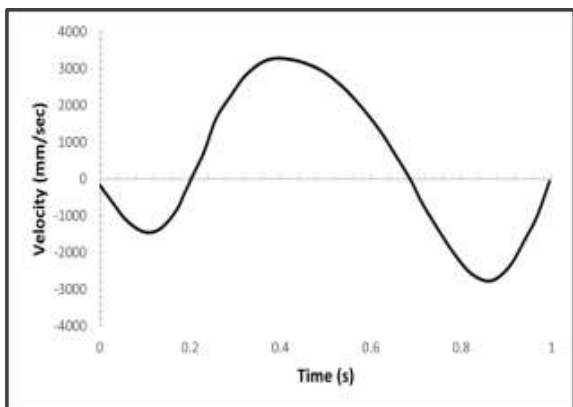


Fig. 45: Coupler point- velocity vs time

The maximum value of velocity obtained from the software is about 3225 mm/s. The trend is much smoother compared to the plot obtained by a real small-scale model analysis. This is because noise and external vibrational effects are not included in the simulation, and only the formula is used to calculate the velocity of the coupler point.

The further integration of the velocity curve with the help of data points in the Matlab code provided the displacement curve of the coupler joint. The coupler point- displacement vs time is presented in Figure 46.

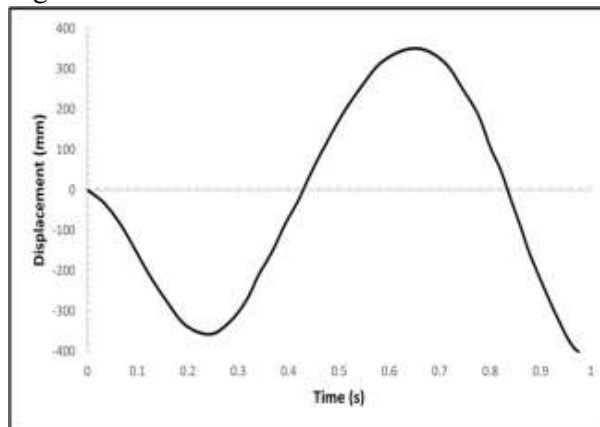


Fig. 46: Coupler point- displacement vs time

### 5.2 Practical Analysis of the Model

After the theoretical analysis using the kinematic equations, the next task is to analyze the practically fabricated model. Sinusoidal variations in kinematic quantities are required to compare with the theoretical model. The testing of the program by a mounting sensor on fabricated four-bar dynamic testing apparatus and the following plots (Figure 47, Figure 48, Figure 49, Figure 50, Figure 51, and Figure 52) by running the program when an AC motor drives the apparatus. Initially, the 80 rpm for the motor was set according to the desired criterion of the four-bar testing.

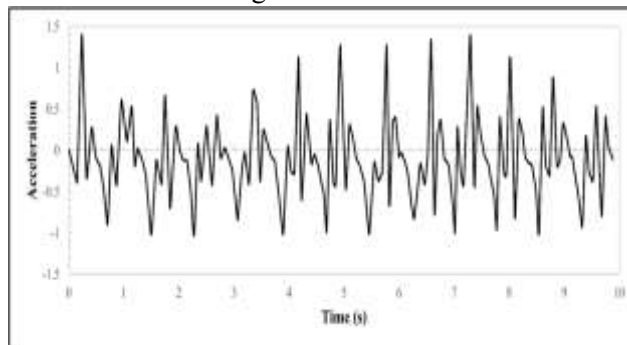


Fig. 47: Coupler point- acceleration vs time at high speed

As shown in the trend of coupler point acceleration in 47, at high speeds, there are many fluctuations,

and the pattern of one complete cycle does not remain the same as a simple sinusoidal pattern. There are maximum and minimum of different magnitudes.

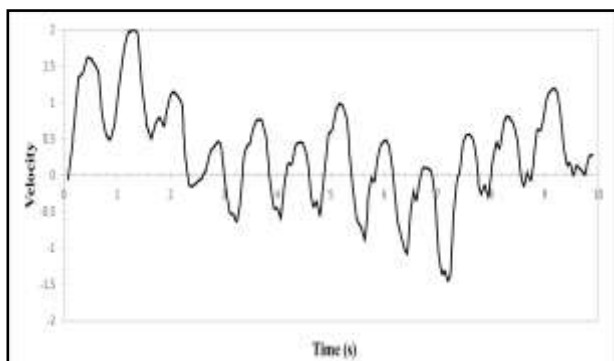


Fig. 48: Coupler point- velocity vs time at high speed

As shown in the trend of coupler point velocity shown in Figure 48, at high speeds, there are many fluctuations, and the pattern of one complete cycle does not remain the same as a simple sinusoidal pattern. There are maximum and minimum of different magnitudes.

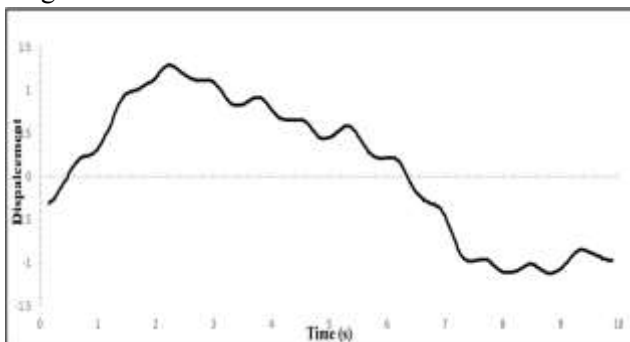


Fig. 49: Coupler point- displacement vs time at high speed

At higher angular speeds, the acceleration plot in Figure 47 shows that during one complete cycle of motion, acceleration goes up and down and is not particularly following a sinusoidal variation. One high peak, two low peaks, and one negative peak occurs during one complete motion cycle. The velocity plot in Figure 48 does not oscillate about the same line, and the graph shifts a little down and again up as more and more motion cycles are completed. This is due to errors in numerical integration. Moreover, this error is magnified and can be seen in the displacement graph in Figure 49. This error looks much due to different scales of Y-axis values for better locomotion of the curve. This analysis at higher rpm suggested a slight change in the cycle pattern compared to the

theoretical analysis for the acceleration curve, which can also be referred to as the impact of noise and vibration. It means that the improvement of the accelerometer can be important to get a similar pattern as obtained in the theoretical model mentioned above. Furthermore, an important step in this regard is to analyze the model's response at the lower rpm of 30 rpm. The following plots were obtained when the procedure was repeated at low speeds (Figure 50):

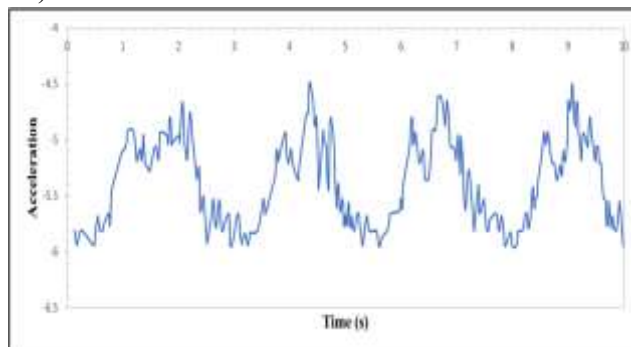


Fig. 50: Coupler point- acceleration vs time at low speed

As can be seen in the trend of coupler point acceleration, there are many fluctuations at low speeds, and the pattern of one complete cycle does not remain the same as a simple sinusoidal pattern. There are sudden and very sharp changes in magnitudes due to noise vibrations. There are maximum and minimum of different magnitudes.

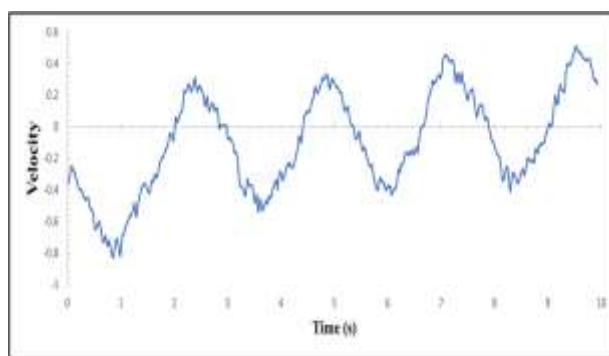


Fig. 51: Coupler point- velocity vs time at low speed

There is a very consistent pattern in coupler point velocity. There are smaller fluctuations that can be neglected. There is a rising pattern in the velocity graph, Figure 51, if more cycles are drawn due to some inherent error causing an offset in integrated data. The coupler point- displacement vs time at low speed is presented in Figure 52.

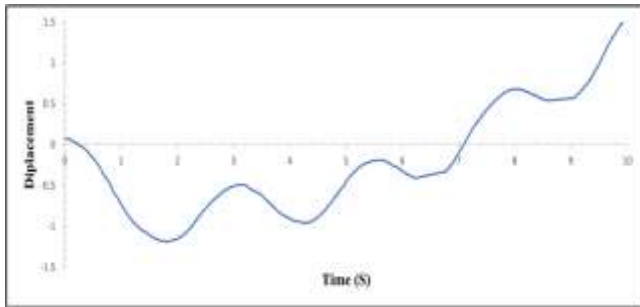


Fig. 52: Coupler point- displacement vs time at low speed

At low speeds, the plots obtained are much clearer than those at high speeds, and one motion cycle can be observed more clearly. However, the plots obtained at low speeds show little deviation about the line of oscillation, and the wave pattern is quite similar to the desired theoretical ones. One reason for this difference is the increase of vibrations at high speeds, which induces acceleration components in any direction in three-dimensional space. The maximum values obtained from the graphs are listed in Table 9.

Table 9. Maximum values of measured dynamic parameters

Angular Velocity, n (rpm)	30	80
Acceleration (m/s <sup>2</sup> )	4.7	17
Velocity (m/s)	0.5	1.7
Displacement (m)	1.35	2.2

The possible reasons for deviations of measured kinematic data using the graphical representation include sudden changes in accelerations, which was because the graph shown could be the result of acceleration vectors in three-dimensional space because actual apparatus had a large mass, with links being relatively heavier compared to small scale model used during initial testing of the program. Moreover, due to a large amount of power transmitted from the motor to the shaft of the crank link, vibrations in a plane perpendicular to the plane of motion of the linkage were induced. The location on the shaft at which power was being transmitted was not in the plane of motion of linkage. Some relevant studies can be found in [31] and [32].

## 6 Results and Discussion

The above portion of program testing and findings vividly explained the performance of four-bar mechanisms at different applied RPMs. A major comparison in this regard is very important between theoretical acceleration and practical acceleration. As explained earlier, the conventional integral model is applied in MATLAB coding to obtain the values and graphical interference of the velocity and displacement by integrating the acceleration values. Therefore, a proper understanding of the four-bar mechanism developed practically can only be analyzed most effectively with the help of acceleration which is taken as the key variable and analyzed in this section in detail. To make this comparison even more effective and realistic according to the modern-day applications of different 4 bar mechanisms, lower-end higher RPMs are also compared explicitly with the theoretical acceleration to understand the impact of rpm. First, let us compare the theoretical and Practical acceleration obtained from our prototype at low rpm. The separate wave patterns have already been mentioned in the above section. However, for this comparison, both wave patterns are accumulated in the same graph, as shown below. The wave pattern of practical acceleration at low rpm is similar to the theoretical acceleration in terms of the wave pattern, but amplitude values are different. Theoretical acceleration has higher values as compared to practical acceleration because practical acceleration is at a lower rpm. It is important, however, to notice that the pattern obtained from the acceleration's sinusoidal curve oscillates symmetrically. Lower RPMs can also provide better results if the noise and vibration are removed with the help of using the counterweights and a better-quality sensor. The comparison of Theoretical Acceleration and Practical Acceleration at low rpm is presented in Figure 53.

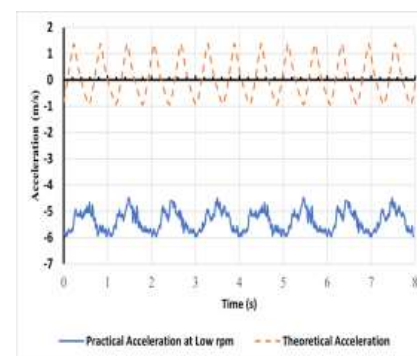


Fig. 53: Comparison of Theoretical Acceleration and Practical Acceleration at low rpm

At this point, it is also important to compare the practical acceleration of the model measured at the higher rpm with the practical acceleration of the model measured at the lower rpm to analyze the attributes of both curves better. The analysis of wave patterns is important to understand the behavior of four-bar mechanisms and their effectiveness compared to the theoretical four-bar mechanism values obtained with the help of theoretical kinematic analysis. The purpose of using higher and lower rpm to analyze the practical acceleration was to include more density in this research so that effective research knowledge can be built and contributed to the people working in dynamic testing machines to understand the rpm requirements.

The comparison of practical acceleration at higher RPM and practical acceleration at lower RPM is put forward to understand how both RPM values impact the overall important variables of the practical acceleration, including amplitude and wavelength as the key variables. It can be vividly observed that the wave pattern of the acceleration curve at the lower rpm is smoother. However, the acceleration curve at the higher rpm provides more similarity to that of the theoretical model. The smoothness of the practical acceleration curve at lower rpm is linked with obtaining better wave patterns with the help of less noise and vibration. On the other hand, the MATLAB values for particle acceleration obtained at higher RPM narrated that they are closer to the values of theoretical acceleration obtained after the theoretical kinematic analysis of four bar mechanism. The comparison of Practical Acceleration at low and High rpm is presented in Figure 54.

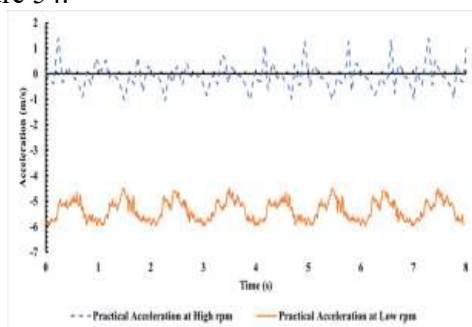


Fig. 54: Comparison of Practical Acceleration at low and High rpm

The next important portion of this discussion is to analyze practical acceleration wave patterns and add lower and higher rpm with the theoretical acceleration. The overall comparison is also

presented to better visualize the situation and the practical and theoretical model responses during the kinematic analysis. The maximum amplitude obtained with the practical model at higher RPMs is the same as that of the theoretical model (The maximum amplitude of practical acceleration is 1.4 m/s and the same as that of the theoretical model 1.4 m/s). It means that, although the smoothness of the curve can be obtained at lower rpm, higher rpm provides both the similarity of amplitude and the wavelength, as explained through the values obtained from the MATLAB model. The comparison of Practical Acceleration at low and high rpm with Theoretical Accelerations is presented in Figure 55.

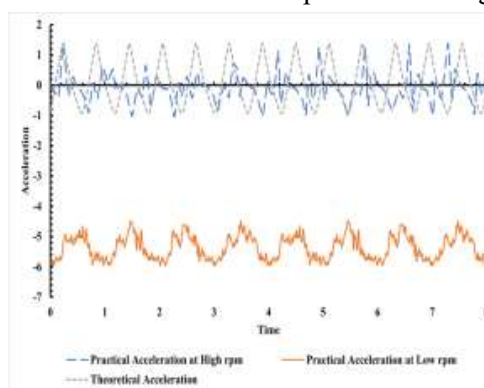


Fig. 55: Comparison of Practical Acceleration at low and high rpm with Theoretical Accelerations

The model, suggested by [32], provides a similar kinematic analysis of the walking machine (robot) kinematics which can be compared with the patterns obtained by our practical model in terms of the acceleration, velocity, and displacement responses. The model for the four-bar kinematic analysis of the waking machine is analyzed at lower RPMs to analyze the robot's motion on the rough terrain requiring less speed for better understanding. Therefore, the maximum acceleration, velocity, and displacement of the model are at different points. The comparison of the model with our desired model narrates that the increased RPMs can provide better results due to less vibration. It is also a matter of fact that the impact of vibration can be countered with the help of adding counterweights. The comparison of our practical acceleration at low and high rpm with theoretical accelerations with the designed model for the analysis of a four-bar walking machine is presented in Figure 56.

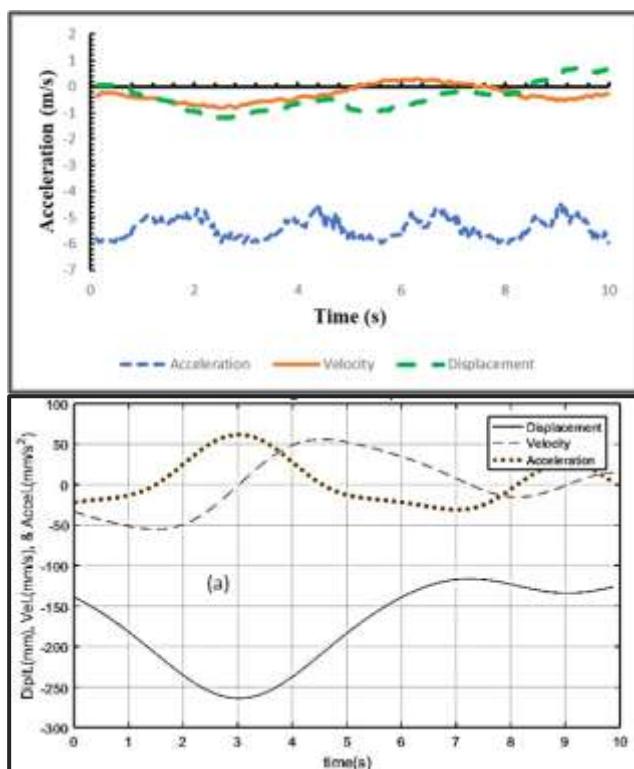


Fig. 56 (a and b): Comparison of our Practical Acceleration at low and high rpm with Theoretical Accelerations with the designed model for the analysis of a four-bar walking machine [32]

The comparison of the wave pattern at the lower and higher RPMs is analyzed with the help of adjusting the higher rpm above the acceleration curve. The adjustment is carried out to analyze better the impact of similar acceleration responses with the theoretical model. It should also be noticed that the theoretical model is impossible to replicate in the four-bar mechanisms' real-time phenomenon due to the involvement of multiple factors like noise, vibration, irregularities in the surface of four bar mechanism, etc. Although the theoretical model is practically impossible to match with the practical acceleration obtained from a practically developed prototype because of many external factors, it can be sought for better motions and the kinematic analysis results. The theoretical model is developed with the help of theoretical kinematic analysis using the equations and formula; therefore, it is the ideal situation. On the other hand, the practical acceleration is obtained with the help of kinematic analysis of the prototype developed for the dynamic testing of four bar mechanism. Therefore, it is not easy to replicate the exact similar values in the practical model using practical acceleration values. It can be analyzed from the graph given below that the maximum amplitude obtained in the cycles till 10 seconds for the curve obtained at the lower

RPMs is 0.5m/s. It means it is way less than the one obtained at the higher rpm. Hence, it can be classified as the optimum choice of the design engineer to optimize the setup and obtain the required results by compromising the other. The comparison of wave-pattern of practical acceleration at low and high rpm with theoretical accelerations is presented in Figure 57.

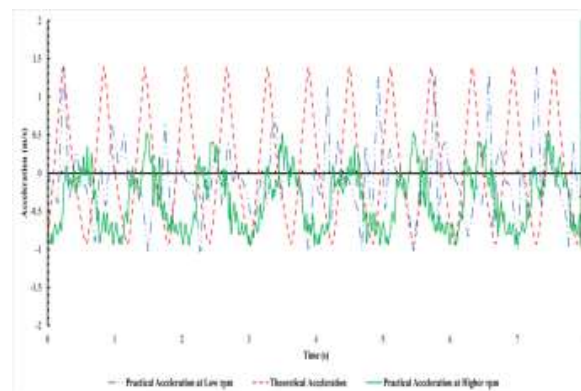


Fig. 57: Comparison of wave-pattern of Practical Acceleration at low and high rpm with Theoretical Accelerations

## 7 Conclusion and Recommendations

### 7.1 Conclusion

In this project, a study of mechanical four-bar linkage was done. The kinematic design of the four-bar mechanism was done by keeping in view the Grashof rotatability criteria, and the dynamic design required factoring in the forces acting on various links, which was used to select the material required for the fabrication of the linkages. The fabrication of the linkages and the assembly of the mechanism was performed. The mounting of the accelerometer sensor, ADXL335, on the mechanism was done to measure accelerations induced in the mechanism due to motion under different angular speeds of the driving motor. Data acquisition was implemented through a microcontroller connected to a computer. The numerical integration was performed using a numerical solver to obtain graphical variations of the velocity and displacement of a specific point on linkage. Errors due to noise and the accuracy of the mathematical method used can be visualized. More accurate plots can be obtained by using more advanced integration techniques and highly sensitive accelerometers and force transducers (piezoelectric sensors) for measurement and instrumentation. The integration, which is used for the accumulation of velocity and displacement from the acceleration obtained from the accelerometer, can be further improved by the mathematical

modeling of that kinematic analysis and incorporating it into the MATLAB code. The more sophisticated model will incorporate more extraneous variables; therefore, advanced integration techniques can provide better results. The same is the case with highly sensitive accelerometers and force traducers because they provide better acceleration values due to better sensitivity than the accelerometer used for this research.

## 7.2 Future Recommendations

The results obtained for the acceleration, velocity, and displacement graphs can be improved. The differences in the graphs obtained using the software and via experiment can be greatly reduced by using a variable frequency drive, which would control the angular velocity (rpm) of the AC motor, along with using more accurate sensors such as accelerometer potentiometer and optical encoder. Moreover, lightweight materials can be used, and shaft and motor coupling can be done through gears (instead of a belt and pulley) to reduce vibrations in the mechanism. Furthermore, a filter can be designed to remove noise in the data obtained from the sensors, which would lead to a reduction in the errors obtained.

### References:

- [1] Al-Jazari, The Book of Knowledge of Ingenious Devices
- [2] Yi Zhang, Introduction to Mechanisms, 1st Edition, Carnegie Mellon University, 2003
- [3] Francis C. Moon, The Machines of Leonardo da Vinci and Franz Reuleaux, 1st Edition, Springer, Dordrecht, 2007.
- [4] Oleg Vinogradov, Fundamentals of Kinematics and Dynamics of Machines and Mechanisms, 1st Edition, CRC Press, 2000
- [5] Acharyya, S. K., & Mandal, M. (2009). Performance of EAs for four-bar linkage
- [6] Mathworks, "Primitive joint with one rotational degree of freedom" URL: <https://www.mathworks.com/help/phymod/s/m/mech/ref/revolute.html>
- [7] Joseph Edward Shigley, John Joseph Uicker, Theory of Machines and Mechanisms, 2nd Edition, McGraw-Hill, 1995
- [8] Kamat, G., Hoshing, G., Pawar, A., Lokhande, A., Patunkar, P., & Hatawalane, S. (2014). Synthesis and analysis of adjustable planar four-bar mechanism. International Journal of Advanced Mechanical Engineering, 4(3), 263-268.
- [9] Metiku, R. (2004). Computer-Aided Dynamic Force Analysis of Four-Bar Planar Mechanisms (Doctoral dissertation, Addis Ababa University).
- [10] Cunkas, M., & Aydoğdu, O. (2010). Realization of fuzzy logic controlled brushless dc motor drives using Matlab/Simulink. Mathematical and Computational Applications, 15(2), 218-229.
- [11] Gündoğdu, Ö., & Erentürk, K. (2005). Fuzzy control of a dc motor driven four-bar mechanism. Mechatronics, 15(4), 423-438.
- [12] Ahmedalbashir, M., Romdhane, L., & Lee, J. (2017). Dynamics of a four-bar mechanism with clearance and springs-Modeling and experimental analysis. Journal of Mechanical Science and Technology, 31(3), 1023-1033.
- [13] Erkaya, S., & Uzmay, I. (2009). Investigation on effect of joint clearance on dynamics of four-bar mechanism. Nonlinear Dynamics, 58(1), 179-198.
- [14] Yildiz, A., Kopmaz, O., & Cetin, S. T. (2015). Dynamic modeling and analysis of a four-bar mechanism coupled with a CVT for obtaining variable input speeds. Journal of Mechanical Science and Technology, 29(3), 1001-1006.
- [15] Noh, J., Kwon, J., Yang, W., Oh, Y., & Bae, J. H. (2016, October). A 4-bar mechanism based for knee assist robotic exoskeleton using singular configuration. In IECON 2016-42nd Annual Conference of the IEEE Industrial Electronics Society (pp. 674-680). IEEE.
- [16] Alfaro, M. E., Bolnick, D. I., & Wainwright, P. C. (2004). Evolutionary dynamics of complex biomechanical systems: an example using the four-bar mechanism. Evolution, 58(3), 495-503.
- [17] McDonald, M., & Agrawal, S. K. (2010). Design of a bio-inspired spherical four-bar mechanism for flapping-wing micro air-vehicle applications.
- [18] Wahit, M. A. A., Ahmad, S. A., Marhaban, M. H., Wada, C., & Izhar, L. I. (2020). 3D Printed Robot Hand Structure Using Four-Bar Linkage Mechanism for Prosthetic Application. Sensors (Basel, Switzerland), 20(15).
- [19] Erkaya, S., & Uzmay, I. (2009). Investigation on effect of joint clearance on dynamics of four-bar mechanism. Nonlinear Dynamics, 58(1), 179-198.

- [20] Chaudhary, Naman, and Arpan Gupta. "Multi-body Analysis for a Four-Bar Mechanism Using RecurDyn and MATLAB." *Machines, Mechanism and Robotics*. Springer, Singapore, 2022. 1813-1823.
- [21] Krašna, S., Ciglaric, I., & Prebil, I. (2002). Four-bar linkage design using global optimization approach. In *DS 30: Proceedings of DESIGN 2002, the 7th International Design Conference, Dubrovnik* (pp. 1199-1204).
- [22] Gupta, K. C., & Ma, R. (1995). A direct rotatability criterion for spherical four-bar linkages.
- [23] Demeulenaere, B., Aertbeliën, E., Verschuure, M., Swevers, J., & De Schutter, J. (2006). Ultimate limits for counterweight balancing of crank-rocker four-bar linkages.
- [24] Arunkumar, N., Santhosh, R., & Subramaniam, S. S. (2014). Infinitely Variable Transmission Using Four Bar Mechanism. *International Journal of Engineering Science and Technology*, 6(4), 170.
- [25] Shigley, *Theory of Machines and Mechanisms, Fifth Edition* 1981
- [26] BBman, "Belt length calculator" URL: <https://www.bbman.com/belt-length-calculator/>
- [27] Dejan Nedelkovski, "How Rotary Encoder Works and How To Use It with Arduino", 25 July 2016 URL: <https://howtomechatronics.com/tutorials/arduino/rotary-encoder-works-use-arduino/>
- [28] Vigen Arakelian, Sébastien Briot, *Balancing of Linkages and Robot Manipulators*, Volume 27, Springer, 2015
- [29] Tang, C. P. (2010). Lagrangian dynamic formulation of a four-bar mechanism with minimal coordinates.
- [30] Guo-you, X. U. (2011). Modification of Crust Breaker Mechanism of Aluminum Electrolysis Multi-Function Unit [J]. *Energy Saving of Nonferrous Metallurgy*, 2.
- [31] Electronic Wings, "ADXL335 Accelerometer Interfacing with Arduino Uno" URL: <https://www.electronicwings.com/arduino/adx335-accelerometer-interfacing-with-arduino-uno>.
- [32] Terefe, T. O., Lemu, H. G., & Tuli, T. B. (2019). Kinematic Modeling and Analysis of a Walking Machine (Robot) Leg Mechanism on a Rough Terrain. *Advances in Science and Technology. Research Journal*, 13(3).

### **Contribution of Individual Authors to the Creation of a Scientific Article (Ghostwriting Policy)**

- Muhammad Maarij, the corresponding author, dealt with the design of four bar mechanism and the numerical analysis of the mechanism using MATLAB.
- Muhammad Ali performed the manufacturing of required parts in the laboratory including all components rocker, coupler, shaft assembly and the counterweights.
- Muhammad Shehryar Manzoor, being the supervisor of the project, supervised the complete procedure and guided with valuable suggestions, and validated the research with the existing articles.

### **Sources of Funding for Research Presented in a Scientific Article or Scientific Article Itself**

Not any source of funding is obtained.

### **Conflict of Interest**

The authors have no conflict of interest to declare.

### **Creative Commons Attribution License 4.0 (Attribution 4.0 International, CC BY 4.0)**

This article is published under the terms of the Creative Commons Attribution License 4.0

[https://creativecommons.org/licenses/by/4.0/deed.en\\_US](https://creativecommons.org/licenses/by/4.0/deed.en_US)